Cross-sectional scanning tunneling microscopy of GaAsSb/GaAs quantum well structures

S. L. Zuo,[a] Y. G. Hong, and E. T. Yu[b]
Department of Electrical and Computer Engineering, University of California, San Diego, La Jolla, California 92093-0407

J. F. Klem
Sandia National Laboratories, Albuquerque, New Mexico 87185

We have used cross-sectional scanning tunneling microscopy (STM) to perform nanometer-scale characterization of compositional structure and interfacial properties within $GaAs_{1-x}Sb_x$/GaAs double-quantum well structures. An algorithm has been devised based on analysis of strain effects in STM data to obtain detailed, quantitative compositional profiles within alloy layers. Using this and other analysis techniques, we have assessed the influence of group V anion soaks at each heterojunction interface on interface roughness and abruptness. An As soak at the GaAs–on–$GaAs_{1-x}Sb_x$ interfaces reduces interface roughness but leads to a slight loss of abruptness at the interface, while an As+Sb soak at $GaAs_{1-x}Sb_x$–on–GaAs interfaces improves abruptness while leaving interface roughness largely unaffected. Significant compositional grading at the nanometer scale is observed within the $GaAs_{1-x}Sb_x$ layers. © *2002 American Institute of Physics.*
[DOI: 10.1063/1.1501740]

I. INTRODUCTION

Optoelectronic devices operating at 1.3 μm are of great importance for optical fiber communications and data link systems. $GaAs_{1-x}Sb_x$-based heterostructures grown on GaAs substrates have shown increasing promise for vertical-cavity surface-emitting lasers operating at 1.3 μm: this material system is compatible with the well-established $AlAs/Al_{1-x}Ga_xAs$ distributed Bragg reflectors and aperture fabrication using oxidation of AlAs. The biaxial compressive strain in $GaAs_{1-x}Sb_x$ alloy layers coherent with GaAs substrates modifies the valence-band structure and facilitates population inversion in laser devices.[1–4]

However, for III-V alloys, compositional features such as ordering, clustering, phase separation, and spontaneous compositional modulation have been observed to occur, and can significantly influence material properties.[5–14] Interface quality within III-V semiconductor heterostructures is also of great importance for optimization of device performance: interface roughness and abruptness at the atomic scale will directly influence carrier confinement, carrier mobility, and photoresponse. To improve interfacial properties, e.g., to reduce interface roughness, various protocols may be employed during the growth of heterojunction interfaces; however, these procedures may also affect other interface properties such as abruptness, compositional profiles, and consequently, electronic and optical properties.

In this article, we describe cross-sectional scanning tunneling microscopy (STM) studies of $GaAs_{1-x}Sb_x$/GaAs quantum well structures grown by molecular-beam epitaxy

(MBE). In the $GaAs_{1-x}Sb_x$/GaAs heterostructures used in our studies, a variety of the effects described above are observed and investigated. Details concerning the experiments and sample structure are described in Sec. II. High-resolution cross-sectional STM images obtained from $GaAs_{1-x}Sb_x$/GaAs double quantum well samples with interfaces grown under a variety of conditions are presented in Sec. III. These images clearly show inhomogeneous compositional structures at the nanoscale in the $GaAs_{1-x}Sb_x$ alloy layer. Interface profiles extracted from STM images illustrate the effects of interface growth conditions on interface roughness. Furthermore, a detailed analysis of strain effects on surface morphology and STM imaging is found to allow extraction of quantitative information on the detailed compositional profiles within the $GaAs_{1-x}Sb_x$ alloy layer. Section IV concludes the article.

II. EXPERIMENT

The $GaAs_{1-x}Sb_x$/GaAs double quantum well samples used in these studies were grown by MBE. Cracking effusion cells were used for As and Sb sources, such that the dominant incident group V species were As_2 and Sb_1. For each sample, a 3000 Å GaAs buffer layer was grown initially on an *n*-type GaAs (001) substrate at 590 °C, followed by a two-period 280 Å GaAs/70 Å $GaAs_{1-x}Sb_x$ quantum well structure grown at 475 °C. Heterojunction interfaces within one sample were treated with a group V soak: a 10 s As + Sb soak for $GaAs_{1-x}Sb_x$–on–GaAs interfaces and a 90 s As soak for GaAs–on–$GaAs_{1-x}Sb_x$ interfaces; the other sample was grown without the anion soaks but otherwise under identical conditions. Figure 1 shows a schematic illustration of the sample structure and STM geometry employed in these studies.

---

[a]Current address: Qualcomm Inc., 5775 Morehouse Dr., San Diego, CA 92121.
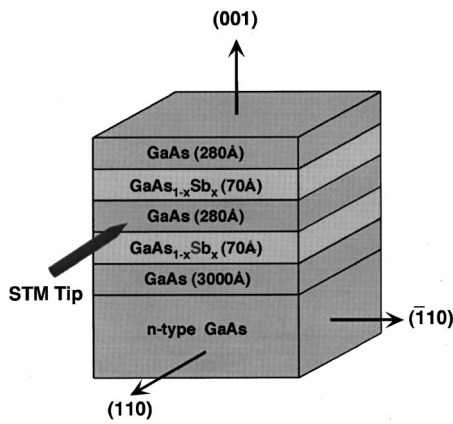[b]Electronic mail: ety@ece.ucsd.edu

FIG. 1. Schematic illustration of the structure of $GaAs_{1-x}Sb_x$/GaAs double quantum well samples and STM geometry used in our studies.

FIG. 2. X-ray diffraction measurements and simulations for $GaAs_{1-x}Sb_x$/GaAs double quantum wells grown (a) with and (b) without group V soaks. The Sb concentration is determined to be 35% and 34%, respectively, within the $GaAs_{1-x}Sb_x$ alloy layer in the $GaAs_{1-x}Sb_x$/GaAs double quantum well heterostructures grown with and without group V soak at interfaces.

Figure 2 shows the x-ray diffraction (XRD) measurements of our two samples, from which we deduce that the average Sb concentration within the $GaAs_{1-x}Sb_x$ alloy layers in our $GaAs_{1-x}Sb_x$/GaAs samples grown with and without group V soaks at the interfaces is 35% and 34%, respectively. Figures 3(a) and 3(b) show the room-temperature photoluminescence (PL) spectra of our two samples grown with and without the group V interface soaks. The PL spectra are centered at 1.25 and 1.26 μm, respectively, corresponding to energies of $\sim$0.99–0.98 eV, and with full widths at half maximum of $\sim$80 meV. To investigate the detailed nanometer-scale compositional and interfacial properties of these samples, cross-sectional STM studies were performed on the (110) cross sections exposed by *in situ* cleaving in an ultrahigh vacuum chamber with a base pressure of $\sim$7 $\times 10^{-11}$ torr. Electrochemically etched W tips and commercially available Pt/Ir tips cleaned *in situ* by electron bombardment were used for these studies.

III. RESULTS AND DISCUSSION

A. Local compositional structure in $GaAs_{1-x}Sb_x$ alloys

Figure 4(a) shows a three-dimensional rendering of a 100 Å$\times$160 Å filled-state (110) constant-current STM image containing one $GaAs_{1-x}Sb_x$ alloy layer and two adjacent GaAs layers in the 70 Å $GaAs_{1-x}Sb_x$/280 Å GaAs structure grown with group V soaks at the heterojunction interfaces, obtained at a sample bias of -2.4 V and a tunneling current of 0.1 nA. The $GaAs_{1-x}Sb_x$ layer appears brighter (higher topographically), while the GaAs layer appears darker (lower topographically), with a typical topographic contrast of $\sim$3.7–4 Å between the two layers. The topographic contrast observed in the filled-state constant-current STM images between the $GaAs_{1-x}Sb_x$ and GaAs layers can arise from two sources:[15] electronically induced contrast and surface modulation of the exposed (110) cross section. First, a pseudomorphic $GaAs_{1-x}Sb_x$/GaAs quantum well grown on a (001) GaAs substrate has a significant valence-band offset, with the valence-band-edge energy of the $GaAs_{1-x}Sb_x$ alloy layer higher than that of the GaAs layer, but the conduction-band offset is very small.[16–18] The valence-band alignment would
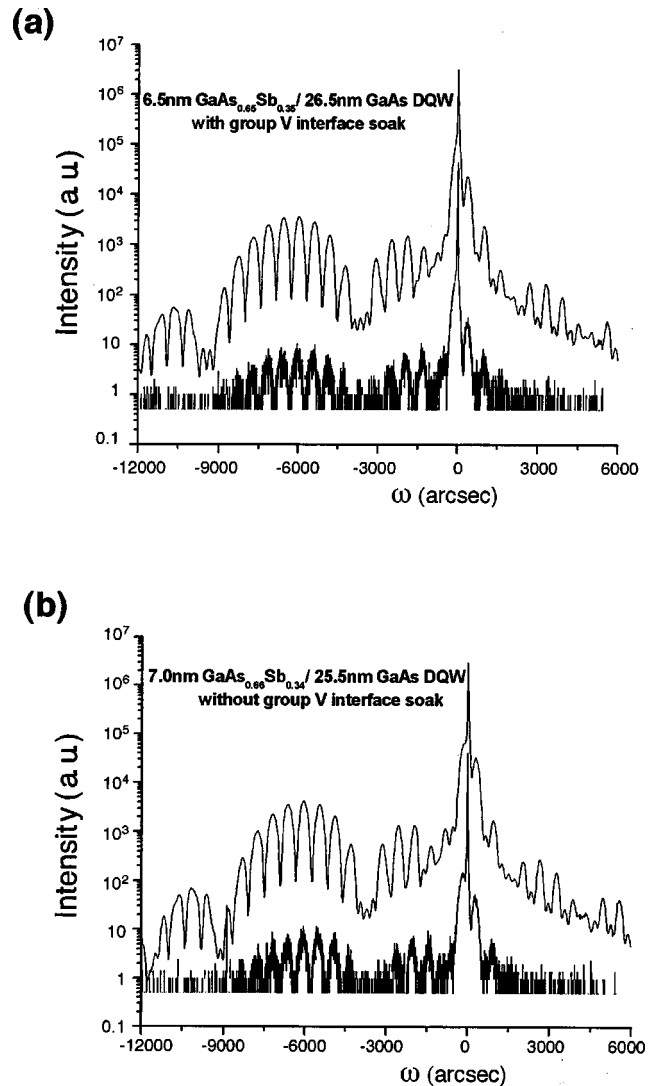
lead to a larger tip-sample separation while acquiring a filled-state constant-current STM image, i.e., greater topographic height, in the $GaAs_{1-x}Sb_x$ layer in a filled-state constant-current STM image. Second, the compressive strain in the $GaAs_{1-x}Sb_x$ layers will lead to actual topographic variation on the cleaved surface—the compressively strained $GaAs_{1-x}Sb_x$ layers will protrude slightly on the exposed (110) cross section. Such morphological variations will also cause the $GaAs_{1-x}Sb_x$ layer to appear higher and the GaAs layers to appear lower topographically. A numerical simulation we have performed of this effect indicates that the amplitude of surface undulation on an exposed (110) surface of the 70 Å $GaAs_{1-x}Sb_x$/280 Å GaAs structure is $\sim$3.5 Å for $x\sim$0.35.

In addition to the overall contrast between the $GaAs_{1-x}Sb_x$ and GaAs layers, detailed nanometer-scale features are clearly visible within the $GaAs_{1-x}Sb_x$ alloy layer. These features arise due to local variations in electronic
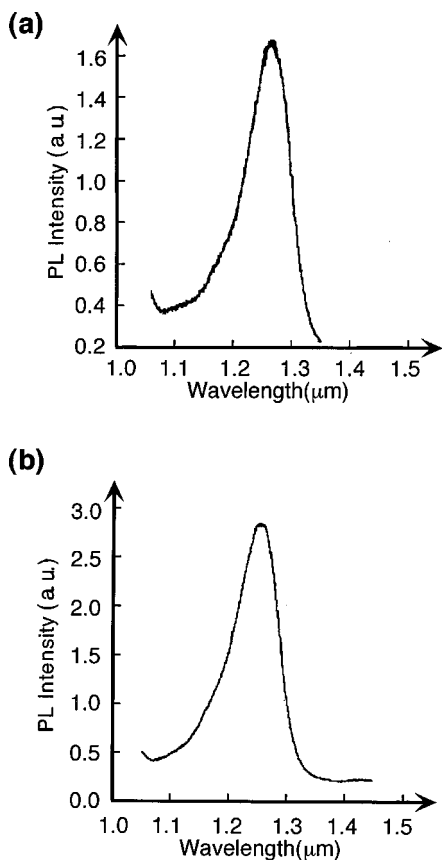
(a)

(b)

FIG. 3. Room-temperature photoluminescence spectra of the GaAs$_{1-x}$Sb$_x$/GaAs double quantum well heterostructures grown (a) with and (b) without group V soak at interfaces.

(a)

(b)

FIG. 4. Three-dimensional rendering of (a) a 100 Å × 160 Å and (b) a 100 Å × 140 Å filled-state (110) constant-current STM images of GaAs$_{1-x}$Sb$_x$/GaAs DQW structure grown with and without group V soaks at the heterojunction interfaces, respectively, obtained at a sample bias of −2.4 V and a tunneling current of 0.1 nA. Arrows indicate major directions and some ⟨112⟩ compositional features within the GaAs$_{1-x}$Sb$_x$ alloy layer.

structure, arising from corresponding fluctuations in compositional structure. Increasing the Sb concentration within a GaAs$_{1-x}$Sb$_x$ alloy layer pseudomorphically grown on a GaAs substrate will raise the GaAs$_{1-x}$Sb$_x$ valence-band edge, and will also increase the compressive strain within the GaAs$_{1-x}$Sb$_x$ alloy layer, leading to greater surface protrusion on the exposed (110) cross section. Therefore, brighter features observed within the GaAs$_{1-x}$Sb$_x$ alloy layer in a filled-state constant-current STM image are unambiguously Sb rich, and darker features are As rich. Nanometer-scale As-rich and Sb-rich regions with features preferentially oriented along the [$\bar{1}$12] and [1$\bar{1}$2] directions in the (110) plane in the GaAs$_{1-x}$Sb$_x$ alloy layer are clearly visible in Fig. 4(a). Such features are indicative of As-rich and Sb-rich regions with boundaries contained within (1$\bar{1}$1) and ($\bar{1}$11) planes,[19] reminiscent of CuPt–B type ordering, the most frequently observed type of ordering within zinc blende III-V semiconductors.

Similar compositional structures within the GaAs$_{1-x}$Sb$_x$ alloy layers are also observed in cross-sectional STM images obtained from the sample grown without anion soaks at the heterojunction interfaces, as shown in Fig. 4(b), a three-dimensional rendering of a 100 Å × 140 Å filled-state constant-current STM image obtained at a sample bias of −2.4 V and a tunneling current of 0.1 nA from a (110) cross

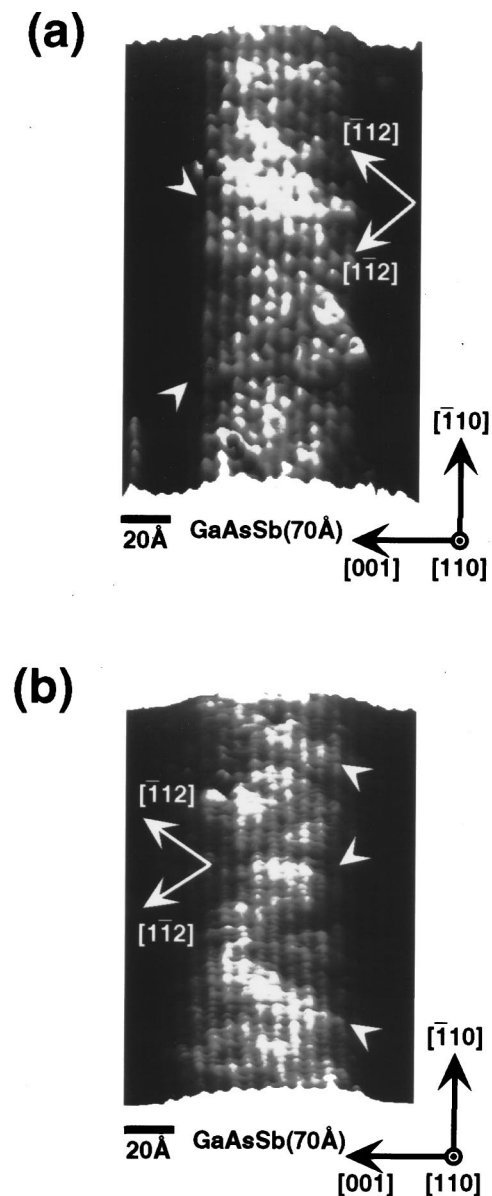section of the GaAs$_{1-x}$Sb$_x$/GaAs sample grown without any interface anion soaks.

Several possible sources of localized compositional variations in alloys have been studied and described previously in the literature. One possible source of the observed compositional variations is spinodal decomposition in the GaAs$_{1-x}$Sb$_x$ alloy layer.[20] Due to the large lattice mismatch (~7.8%) between GaAs and GaSb, compositional variations within a pseudomorphic GaAs$_{1-x}$Sb$_x$ alloy layer lead to additional elastic energy. For cubic crystals, when the elastic moduli satisfy $2C_{44} - C_{11} + C_{12} > 0$, the elastic energy associated with the periodic compositional wave of spinodal decomposition would be minimized if the compositional varia-

tion is oriented along the $\langle 100 \rangle$ directions and maximized for periodicity along the $\langle 111 \rangle$ directions.[21] For our GaAs$_{1-x}$Sb$_x$ alloy, we have $2C_{44} - C_{11} + C_{12} > 0$; therefore, the compositional features observed within the GaAs$_{1-x}$Sb$_x$ alloy layers most likely do not correspond to pure spinodal decomposition within the bulk material.

Theoretical studies of compositional features within alloys have shown that growth kinetics can be a key factor in determination of the compositional structures that form for nonequilibrium growth techniques such as MBE. Compositional structures that correspond to lower Gibbs free energy, and processes that reduce the total Gibbs free energy of the material system, will be favored. Theoretical models of ordering in III-V alloys have suggested that alloy ordering can arise from strain-induced order in surface reconstructions present during growth that is subsequently incorporated into the structure of the epitaxially grown alloy.[22–24] This phenomenon gives rise to near-surface ordered structure, since an ordered structure beneath the reconstructed growth surface yields a lower Gibbs free energy than a random alloy, even though the Gibbs free energy of the ordered structure is generally higher than that of the random alloy in bulk.[10] The resulting ordered structure can then be retained as additional material is grown.

Strain is also a significant factor that affects growth kinetics when there is a significant lattice mismatch between the binary components of a III-V alloy, and can arise from both local compositional variations and lattice mismatch with the substrate.[25–28] In such cases, there exist elastic interactions among regions of differing composition and between these regions and the substrate, resulting in additional elastic energy associated with such compositional features.[25–28] Such elastic energy can constitute a significant component of the total Gibbs free energy and the tendency to reduce the total Gibbs free energy can significantly affect the growth kinetics, resulting in local variations in compositional structure of III-V alloys.[25–28] Theoretical studies have shown that infinite-range elastic interactions play a very important role in the formation and evolution of compositional structures and often result in nanometer-scale compositional features corresponding to a mixture of an ordered structure and disordered phase separation, which usually possess diagonal preferential orientation in cubic compound semiconductors.[25–28]

The compositional structures we observe within the GaAs$_{1-x}$Sb$_x$ alloy layers in Figs. 4(a) and 4(b), with preferential orientations along the $[1\bar{1}2]$ and $[\bar{1}12]$ diagonal directions in the exposed (110) cross-sectional plane, are consistent with the theoretical models suggested above for compositional ordering induced by surface reconstruction, and with models of nanometer-scale compositional features formed under the influence of elastic interaction among regions of differing composition and between these regions and the substrate.

B. Heterojunction interface roughness

High-resolution STM images also allow detailed analysis of interface roughness,[29] and its dependence in our stud-
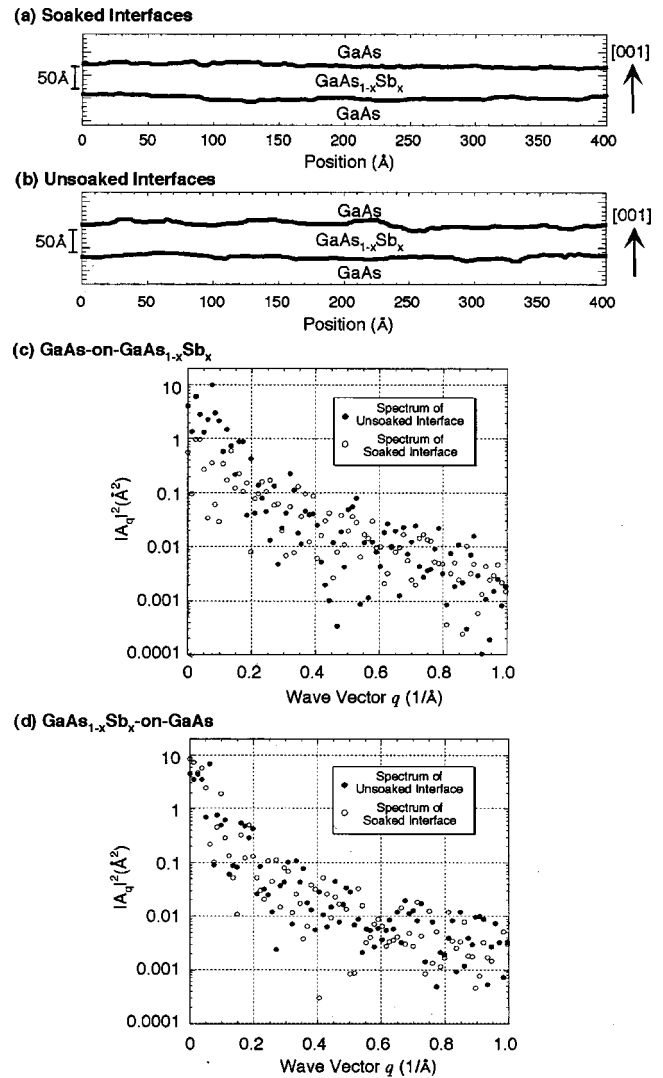

FIG. 5. Interface profiles extracted from (110) cross-sectional STM images obtained from GaAs$_{1-x}$Sb$_x$/GaAs DQW samples grown (a) with and (b) without group V soak at heterojunction interfaces, respectively. Interface power spectra for GaAs–on–GaAs$_{1-x}$Sb$_x$ and GaAs$_{1-x}$Sb$_x$–on–GaAs interfaces, treated with group V soak and untreated, are shown in (c) and (d).

ies on interface anion soaks. GaAs–on–GaAs$_{1-x}$Sb$_x$ and GaAs$_{1-x}$Sb$_x$–on–GaAs interface profiles were extracted, using image-processing techniques described previously,[30] from GaAs$_{1-x}$Sb$_x$/GaAs samples grown with and without interface anion soaks, as shown in Figs. 5(a) and 5(b). Discrete Fourier transforms were performed on these interfaces, yielding the power spectra shown in Figs. 5(c) and 5(d).

The effects of interface roughness, e.g., carrier mobility reduction by interface roughness scattering or broadening of PL linewidths, are typically determined by Fourier components of interface roughness at wavelengths comparable to parameters such as the Fermi wavelength (for carrier transport) or the exciton radius (for luminescence), and hence are dominated by low-frequency spectral components.[30] Therefore, the influence of interface roughness can be assessed by considering the magnitudes of Fourier components as a function of wave vector, particularly in low-frequency range. Examining the power spectra shown in Fig. 5(c), it is apparent

that for wave vectors below ~0.2 Å^{-1}, the Fourier amplitude for roughness of the GaAs–on–GaAs$_{1-x}$Sb$_x$ interface in the GaAs$_{1-x}$Sb$_x$/GaAs sample grown with group V interface soaks (denoted by open circles) is several times smaller than that of the GaAs–on–GaAs$_{1-x}$Sb$_x$ interface in the sample grown without interface soaks (denoted by solid circles). Therefore, within the (110) plane, the anion soaked GaAs–on–GaAs$_{1-x}$Sb$_x$ interface is much smoother than the GaAs–on–GaAs$_{1-x}$Sb$_x$ interface grown without interface soak. While in Fig. 5(d), the Fourier spectra of the anion soaked GaAs$_{1-x}$Sb$_x$–on–GaAs interfaces (denoted by open circles) and those of the unsoaked GaAs$_{1-x}$Sb$_x$–on–GaAs interfaces (denoted by solid circles) are mixed throughout the wave-vector range from 0 to 1 Å^{-1}, therefore, for the GaAs$_{1-x}$Sb$_x$–on–GaAs interfaces, the anion soaks do not appear to yield any significant reduction in interface roughness within the (110) plane.

C. Analysis of atomic bilayer spacing in STM images

Continuum elasticity theory has been shown to be valid at dimensions as small as one atomic layer in III-V compounds,[31–33] and may therefore be used to analyze high-resolution STM images to obtain detailed information concerning the nanometer-scale compositional structure within alloy layers, interface properties, and the effects of treatments such as anion soaks on compositional and interfacial properties. To apply such an analysis to cross-sectional STM images, however, it is necessary to analyze in detail the effect of local strain, strain relaxation, STM tip convolution, and possible dangling-bond reorientation on the relaxed exposed cross section on atomic-scale STM contrast.

In filled-state constant-current cross-sectional STM images, local maxima in STM contrast correspond to local maxima in the density of states on the exposed cross-sectional surface; for the filled-state images analyzed in the present studies, these features correspond to dangling bonds of surface group V atoms. The following analysis demonstrates that the [001] spacings between adjacent local maxima in a high-resolution cross-sectional STM image are determined by the [001] bilayer spacings between surface group V atoms, which are, in turn, uniquely determined by the compositional profile of the heterostructure.

Figure 6(a) schematically illustrates the STM coordinate system, the crystal coordinate system, and the coordinates of local maxima in the density of states of the filled dangling bonds and related surface group V atoms within the STM and crystal coordinate systems. The [001] spacing between adjacent local maxima in the density of states of filled dangling bonds projected onto the STM coordinate system, i.e., the difference in X coordinate of contrast maxima, $\Delta_{001}^{STM} = \Delta X_{001}^{STM} = X_2^{STM} - X_1^{STM}$, differs from the [001] spacing between adjacent local maxima in the density of states of dangling bonds along the x axis of the crystal coordinate system, $\Delta_{001}^b = \Delta x^b = x_2^b - x_1^b$, by a relative error

$$\delta_1 = \left| \frac{\Delta_{001}^{STM} - \Delta_{001}^b}{\Delta_{001}^b} \right| \approx |L \cos \theta_1 - L \cos \theta_2|/(L \cos \theta_2)$$

$$= 2 \sin[(\theta_1 - \theta_2)/2] \times \sin[(\theta_1 + \theta_2)/2]/\cos \theta_2, \quad (1)$$
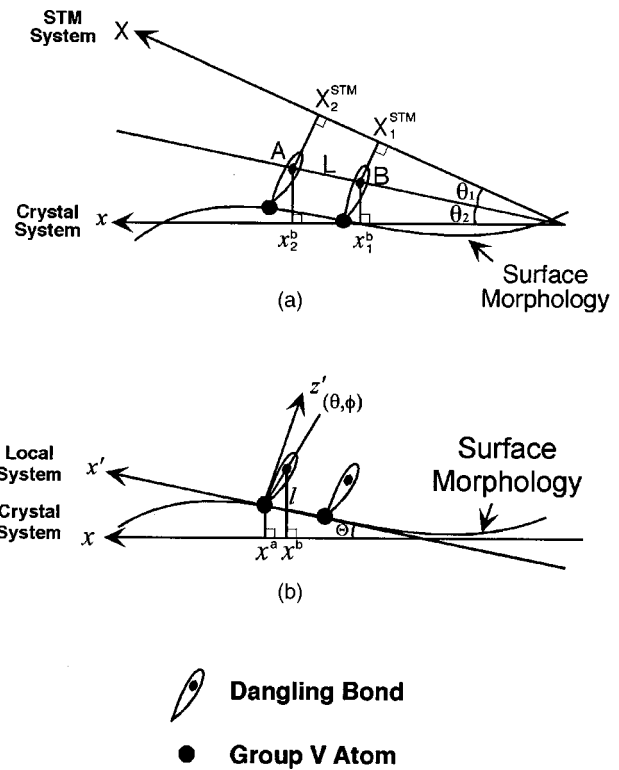

FIG. 6. (a) Schematic illustration of the STM coordinate system, crystal coordinate system, and the coordinates of two adjacent dangling bonds and their corresponding surface group V atoms within the two coordinate system. (b) Schematic illustration of the crystal coordinate system, local coordinate system bound with a surface group V atom, and its associated dangling bond.

where θ_1 is the angle between the x axis of the STM coordinate system and the line segment $\overline{AB}$ connecting two adjacent local maxima in the density of filled states, θ_2 the angle between the line segment $\overline{AB}$ and the x axis of the crystal coordinate system, and L the length of the segment $\overline{AB}$. Both raw STM data and strain simulation show that θ_1 and θ_2 are on the order of ~10^{-2} or smaller, so we obtain $\delta_1 \lesssim 10^{-4}$. In other words, the measured spacing between local maxima in the surface density of states due to filled dangling bond states differ from the actual spacing by at most one part in 10^{-4}.

The [001] spacing along the x axis of the crystal coordinate system between two adjacent filled dangling bonds can then be related to the [001] bilayer spacing between corresponding surface group V atoms along the x axis of the crystal coordinate system. For a group V surface atom and the density-of-states maximum associated with its filled dangling bond, as shown in Fig. 6(b), the difference between their x coordinates is

$$x^b - x^a = l \times (\sin \Theta \cos \theta + \cos \Theta \sin \theta \cos \phi), \quad (2)$$

where θ and ϕ are the polar and azimuthal angles, respectively, of the dangling bond with respect to the local polar coordinate system centered at the surface atom, l is the length of the dangling bond, and Θ the angle between the x axis of the crystal coordinate system and the x' axis of the local polar system, which is determined by the surface morphology of the relaxed cross section. Since Θ, θ, and ϕ de-

pend on the local atomic composition, the average of $x^b - x^a$ for a given surface atom and its dangling bond can be calculated within a random cluster[34–36] centered at the group V surface atom under consideration and extended to the second nearest neighbors, for given local surface morphology and local group V composition. Within such a random cluster, each group V atomic site is occupied by either an As or an Sb atom with a probability determined by the local group V composition. Therefore,

$$
\begin{aligned}
\overline{x^b - x^a} \\
= \sum_{\Omega} \, l(\sin\Theta\cos\theta + \cos\Theta\sin\theta\cos\phi)P_{\Omega}([\mathrm{Sb}])
\end{aligned}
$$

$$
\cong \cos\Theta \times \left(\sum_{\Omega} \, l\sin\theta\cos\phi P_{\Omega}([\mathrm{Sb}]) \right) + \sin\Theta
$$

$$
\times \left(\sum_{\Omega} \, l\cos\theta P_{\Omega}([\mathrm{Sb}]) \right), \tag{3a}
$$

where P_{Ω} is the probability that a certain compositional configuration Ω of the random cluster appears, which is a function of the local Sb concentration [Sb]. Since Θ is very small ($\sim 10^{-2}$ or smaller), we can also define $f_1([\mathrm{Sb}]) \equiv \Sigma_{\Omega} l\sin\theta\cos\phi P_{\Omega}([\mathrm{Sb}])$ and $f_2([\mathrm{Sb}]) \equiv \Sigma_{\Omega} l\cos\theta P_{\Omega}([\mathrm{Sb}])$ in Eq. (3a), to obtain, to the first order in Θ,

$$
\begin{aligned}
\overline{x^b - x^a} \\
\approx \sum_{\Omega} \, l\sin\theta\cos\phi P_{\Omega}([\mathrm{Sb}]) + \Theta
\end{aligned}
$$

$$
\times \left(\sum_{\Omega} l\cos\theta P_{\Omega}([\mathrm{Sb}]) \right)
$$

$$
\equiv f_1([\mathrm{Sb}]) + \Theta \times f_2([\mathrm{Sb}]). \tag{3b}
$$

In areas, where [Sb] changes slowly, i.e., away from the vicinity of heterojunction interfaces, for two adjacent surface group V atoms aligned along the [001] direction and their corresponding dangling bonds, we obtain

$$
\overline{\Delta x^b} - \overline{\Delta x^a} = \overline{\Delta(x^b - x^a)} \cong \Delta\Theta \times f_2([\mathrm{Sb}]), \tag{4}
$$

where Δx^b and Δx^a denote the [001] spacing along the x axis between adjacent-filled dangling bonds, and between their associated group V surface atoms, respectively. Since θ is very small, $f_2([\mathrm{Sb}]) \equiv \Sigma_{\Omega} l\cos\theta P_{\Omega}([\mathrm{Sb}]) \approx \Sigma_{\Omega} l P_{\Omega}([\mathrm{Sb}]) = \bar{l}$, and it is estimated to be slightly greater than 1 Å. Typically, $\Delta\Theta < 10^{-2}$, so the difference between the spacing between adjacent-filled dangling bond states and the spacing between the corresponding surface atoms is ~ 0.01 Å or smaller.

Relaxation at the (110) surface will also affect the coordinates of surface atoms. For zinc-blende III-V crystals cleaved to expose a {110} plane, surface relaxation will occur even when the materials are not strained.[37–39] Surface atoms will shift both within and perpendicular to the local surface morphology, i.e., along the x'' and z'' axes of the local coordinate system, as shown schematically in Fig. 7(a). However, the resulting shifts along the x axis of the crystal coordinate system are very small in absolute value, and *the difference* in such shifts from atom to atom on the exposed surface, which is the factor that affects the measured [001] atomic bilayer
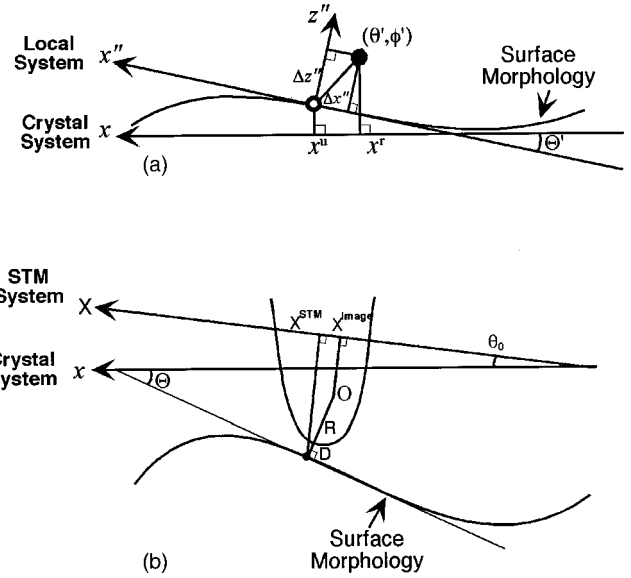

FIG. 7. Schematic illustrations of (a) positions of surface atoms before (circle) and after (solid dot) the (110) surface relaxation with respect to local coordinate system and crystal system, and (b) convolution of STM tip with the sample being imaged.

spacings, is much smaller. For bulk binary materials or random alloys, either free standing or uniformly strained, the relaxation of (110) surfaces will result in uniform horizontal shifts along the x axis of the crystal coordinate system, and hence, will not affect the measured [001] atomic bilayer spacing.

In our studies, local Sb concentration, local strain, and local surface morphology will also affect the relaxation of the (110) surfaces. The average shift along the x axis for a particular surface atom due to the (110) surface relaxation can also be calculated within a random cluster[34–36] and is given by

$$
\begin{aligned}
\overline{x^r - x^u} \\
= \sum_{\Omega} \, (\Delta x''\cos\Theta' + \Delta z''\sin\Theta')P_{\Omega}([\mathrm{Sb}])
\end{aligned}
$$

$$
\approx \overline{\Delta x''} + \Theta'\overline{\Delta z''}, \tag{5}
$$

where x^u and x^r denote the x coordinates of a surface group V atom before and after the (110) surface relaxation, $\Delta x''$ and $\Delta z''$ the shifts of the surface group V atom along the x'' and z'' axes of the local polar coordinate system due to the (110) surface relaxation, and Θ' the angle between the x axis of the crystal coordinate system and the x'' axis of the local coordinate system, as shown in Fig. 7(a). Note that now the local coordinate system is associated with the virtual position of the surface group V atom before the (110) surface relaxation; P_{Ω}, Ω, and [Sb] are defined as in Eq. (3a) and Eq. (4). $\Delta x''$ and $\Delta z''$ are very small, e.g., $\Delta z''$ is usually around 0.2 Å.[37,40–42] For two adjacent surface group V atoms aligned along the [001] direction, the average difference in their shifts along the x axis during the (110) surface relaxation, therefore, is

$$
\overline{\Delta x^r} - \overline{\Delta x^u} = \Delta(\overline{x^r - x^u}) \approx \Delta\Theta'\overline{\Delta z''} \approx \Delta\Theta\overline{\Delta z''}, \tag{6}
$$

assuming that the (110) surface relaxation would not change the morphology of the surface, i.e., $\Delta\Theta \approx \Delta\Theta'$, where $\Delta\Theta$ is

defined in Eq. (4) and is typically less than 0.01. Thus, strain relaxation at the cleaved (110) surface will alter the spacing between adjacent surface atom by less than 0.002 Å.

While imaging the undulated (110) morphology, the shape of the STM tip and the STM contrast (tip-sample separation) will also affect the measured [001] atomic bilayer spacing, as schematically illustrated in Fig. 7(b). Assuming a spherical shape for the STM tip at the apex, for a given point on the exposed (110) surface of the sample, its X coordinate, X^{image}, as perceived by STM tip, differs from its real X coordinate in the STM system according to

$$X^{\text{image}} - X^{\text{STM}} = -(R+D)\sin(\Theta - \theta_0), \tag{7a}$$

where R is the radius of curvature of the tip apex, D the STM tip-sample separation, Θ the angle between the local surface tangent and the x axis of the crystal system, and θ_0 the angle between the X axis of the STM system and the x axis of the crystal system, which is a constant throughout imaging. Therefore, the measured [001] spacings in STM images are affected by the shape of the STM tip and the STM tip-sample separation according to

$$\Delta X_{001}^{\text{image}} - \Delta X_{001}^{\text{STM}} = -\Delta[(R+D)\sin(\Theta - \theta_0)]. \tag{7b}$$

Since Θ and θ_0 are very small, we have,

$$\Delta X_{001}^{\text{image}} - \Delta X_{001}^{\text{STM}} \approx -\Delta[R'(\Theta - \theta_0)], \tag{7c}$$

where $R' = R+D$. R is a constant, typically a few nanometers, D is usually a few angstroms and varies very little in regions away from heterojunction interfaces, and $D \ll R'$, therefore R' is mainly determined by R, and is virtually constant away from heterostructure interfaces. Furthermore, θ_0 is a constant; thus, in regions away from the immediate vicinity of heterostructure interfaces, we obtain

$$\Delta X_{001}^{\text{image}} - \Delta X_{001}^{\text{STM}} \approx -R'\Delta(\Theta - \theta_0) = -R'\Delta\Theta. \tag{7d}$$

From the preceding analysis, we can now establish the quantitative relationships among the following: $\Delta X_{001}^{\text{image}}$, the density-of-state maximum obtained from our STM image data; $\Delta X_{001}^{\text{STM}}$, the actual position of that maximum in the STM coordinate system; x^b, the position of that maximum in the local crystal coordinate system; $x^a = x^r$, the position of the corresponding atom on the relaxed (110) surface; and x^u, the position that atom would assume on the unrelaxed cleaved (110) surface. The local composition can then be determined from x^u as described below.

Using this analysis, we see first that the surface atomic bilayer spacing along the [001] direction before the intrinsic relaxation of the exposed (110) surface (not the strain induced relaxation) is related to the [001] spacings between adjacent maxima in STM contrast in (110) cross-sectional STM images as follows:

$$\Delta X_{001}^{\text{image}} \approx \Delta X_{001}^{\text{STM}} - R'\Delta\Theta$$

$$\approx \overline{\Delta x^b} - R'\Delta\Theta$$

$$\approx \overline{\Delta x^a} + \Delta\Theta\overline{f_2([\text{Sb}])} - R'\Delta\Theta$$

$$\approx \overline{\Delta x^u} + \Delta\Theta\overline{\Delta z''} + \Delta\Theta\overline{f_2([\text{Sb}])} - R'\Delta\Theta$$

$$\approx \overline{\Delta x^u} - R''\Delta\Theta, \tag{8}$$

where $R'' = R' - \overline{\Delta z''} - \overline{f_2([\text{Sb}])} = R + D - \overline{\Delta z''} - \overline{f_2([\text{Sb}])}$, and $\Delta X_{001}^{\text{image}}$, $\Delta X_{001}^{\text{STM}}$, R', Θ, $\overline{\Delta x^b}$, $\overline{\Delta x^a}$, $\overline{f_2([\text{Sb}])}$, $\overline{\Delta x^u}$, and $\overline{\Delta z''}$ are defined in Eq. (1) through Eq. (7). Since $\overline{f_2([\text{Sb}])} \sim 1$ Å, $\overline{\Delta z''} \approx 0.2$ Å, and D is typically couple of angstroms, R'' is slightly larger than R, typically by ~ 1 Å.

In the vicinity of a heterojunction interface, there may be deviations from the above analysis due to the relatively abrupt changes in composition near the interface. These deviations will result in additional uncertainties in the approximated [001] surface atomic bilayer spacing near heterojunction interfaces. However, any increase in the [001] atomic bilayer spacing should be compensated for by a corresponding decrease in the [001] atomic bilayer spacing in the immediate vicinity, and *vice versa*, since the total spacing across the interface is determined by strain relaxation and intrinsic (110) surface relaxation, and abrupt atomic scale compositional variation will only reallocate bilayer atomic spacing near the interface but will not change the total multiple bilayer spacing. Therefore, anomalous deviations can be detected by examining the variation in the [001] atomic bilayer spacing for several bilayers across heterojunction interfaces.

For a given compositional profile in a heterostructure, the surface [001] atomic bilayer spacings are uniquely determined, and the surface [001] atomic bilayer spacing before the intrinsic (110) surface relaxation, $\overline{\Delta x^u}$, can be calculated via numerical simulation of strain effects. If R'' can be determined, either directly or indirectly, the surface [001] spacing between maxima in STM contrast, $\Delta X_{001}^{\text{image}}$, can then be calculated. Therefore, using (i) the [001] spacings measured between adjacent contrast maxima in a STM image, (ii) an independent determination of average composition, e.g., an XRD measurement, and (iii) a numerical simulation of surface relaxation due to strain, the nanoscale compositional profile in the GaAs$_{1-x}$Sb$_x$ alloy layer in our samples can then be determined quantitatively.

D. Quantitative analysis of local atomic composition

The algorithm described in Sec. III C is the first that has been suggested that permits a quantitative analysis of the alloy composition of nanometer-scale compositional structures based on strain analysis of STM data. According to the analysis of Sec. III C, the [001] atomic bilayer spacing on the exposed (110) surface of the GaAs$_{1-x}$Sb$_x$/GaAs heterostructures, $\Delta_{001}^{\text{alloy}}$ and $\Delta_{001}^{\text{GaAs}}$, can be determined using $\Delta_{001}^{\text{image}}$ measured in the corresponding regions within a (110) cross-sectional STM image. R'' is an unknown parameter, but using an XRD measurement to obtain the average Sb concentration within the GaAs$_{1-x}$Sb$_x$ alloy layer, and a numerical simulation to determine the degree of strain-induced surface relaxation, the detailed compositional profiles within the GaAs$_{1-x}$Sb$_x$ alloy layer can then be deduced. Information regarding the abruptness of heterojunction interfaces can be also extracted from the [001] atomic bilayer spacings derived from the interface regions.

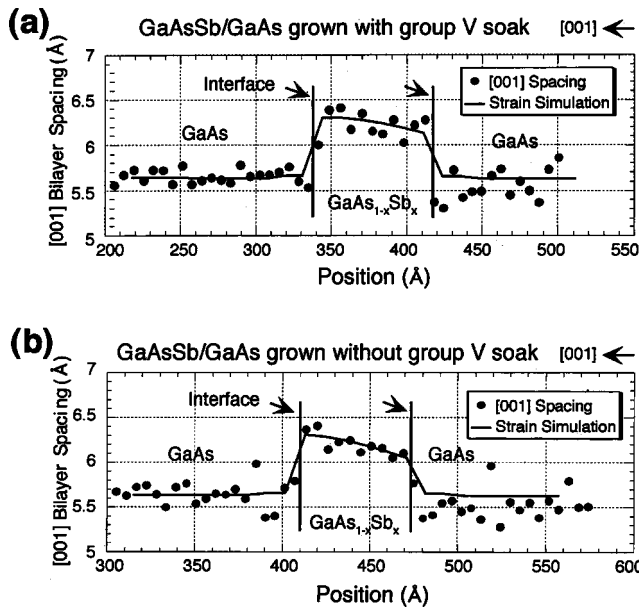The closed circles in Figs. 8(a) and 8(b) show the [001]

(a)

(b)

FIG. 8. [001] atomic bilayer spacings extracted from (110) cross-sectional STM images obtained from $GaAs_{1-x}Sb_x$/GaAs double quantum well samples grown (a) with and (b) without group V soaks at heterojunction interfaces, and results of strain simulation.

atomic bilayer spacings averaged over a distance of 140 Å along the $[\bar{1}10]$ direction in two (110) cross-sectional filled-state constant-current STM images obtained from the $GaAs_{1-x}Sb_x$/GaAs samples grown with and without group V soaks at the heterojunction interfaces, each containing one $GaAs_{1-x}Sb_x$ alloy layer and two adjacent GaAs layers.

It is apparent from Figs. 8(a) and 8(b) that the average [001] spacings vary within the $GaAs_{1-x}Sb_x$ alloy layer, in a manner suggesting that the Sb concentration is significantly graded. As was shown in Fig. 2, the average Sb concentration within the $GaAs_{1-x}Sb_x$ alloy layer in the $GaAs_{1-x}Sb_x$/GaAs samples grown with and without group V soaks at the heterojunction interfaces is determined from XRD measurements to be 35% and 34%, respectively. With this information, a strain simulation was used to determine quantitative compositional profiles within the $GaAs_{1-x}Sb_x$ alloy layer in the two $GaAs_{1-x}Sb_x$/GaAs double quantum samples grown with and without group V interface soaks.

The solid lines in Figs. 8(a) and 8(b) show the results of our strain simulations ($R''\Delta\Theta$ is calculated only for the alloy layer). For a given compositional profile of the alloy layer, Δx^u is calculated, and $\Delta\Theta$ is determined over the alloy layer. From the accumulated discrepancy between ΔX_{001}^{image} and Δx^u throughout the alloy layer, R'' was determined, and the tip convolution was calculated for the alloy layer. Table I lists the maximum, average, and minimum Sb concentration, and the gradient of Sb concentration, within the $GaAs_{1-x}Sb_x$ alloy layer in the $GaAs_{1-x}Sb_x$/GaAs samples grown with and without group V interface soaks. Also listed in Table I are values for R'', and the estimated values for R, the radius of curvature of the STM tip used for acquiring the corresponding STM images.

As shown in Table I, the Sb concentration in the alloy layer is ~30% near the $GaAs_{1-x}Sb_x$–on–GaAs interface, and ~40% near the GaAs–on–$GaAs_{1-x}Sb_x$ interface, with an average Sb concentration of 35% and a group V compositional grading of ~1.5% per nanometer within the alloy layer in the $GaAs_{1-x}Sb_x$/GaAs double quantum wells grown with group V soak; the radius of curvature of the STM tip is estimated to be ~23 Å, based on the value of R''. Within the $GaAs_{1-x}Sb_x$ alloy layer in the $GaAs_{1-x}Sb_x$/GaAs sample grown without group V interface soaks, the Sb concentration in the alloy layer is ~27% near the $GaAs_{1-x}Sb_x$–on–GaAs interface, and ~41% near the GaAs–on–$GaAs_{1-x}Sb_x$ interface, with an average Sb concentration of 34% and a group V compositional grading of ~2% per nanometer; the radius of curvature of the STM tip is estimated in this case to be ~21 Å. The compositional grading in the alloy layer is a direct consequence of Sb segregation during growth, and our results indicate that the group V soaks can significantly reduce the compositional grading caused by the Sb segregation during growth.

The Sb concentrations determined from our analysis within the $GaAs_{1-x}Sb_x$ alloy layer in the $GaAs_{1-x}Sb_x$/GaAs samples grown with and without group V interface soaks, i.e., 30%–40% and 27%–41% respectively, correspond to PL peak energies of ~1 eV at room temperature, consistent with the room temperature PL peak energies measured for these samples.

The data shown in Fig. 8 can also provide information at the nanometer scale concerning local Sb concentration and heterojunction interface abruptness. The degree to which interface abruptness can be probed in this approach is limited by the size of the area used to obtain averaged atomic bilayer spacings and the degree of interface roughness. As shown in Fig. 5, the interface roughness amplitude in these samples is typically about 3 to 8 Å. Since interface roughness is present at length scales comparable to the dimension of the area over which atomic bilayer spacings were averaged to obtain the data shown in Fig. 8, the extent of the interface region in the growth direction will be at least as large as the interface roughness amplitude even if the interface at any single point is perfectly abrupt. However, the actual interface transition region will not be wider than that reflected in the average [001] atomic bilayer spacings. Also, due to the geometry of

TABLE I. Results of strain simulation.

Sample	Maximum [Sb] (%)	Average [Sb] (%)	Minimum [Sb] (%)	Compositional gradient (1/nm) (%)	R'' (Å)	R (Å)
With group-V soaks	40	35	30	1.5	24.3	~23
Without group-V soaks	41	34	27	2	21.6	~21

J. Appl. Phys., Vol. 92, No. 7, 1 October 2002

Zuo *et al.* 3769

the exposed (110) cross section, only the [001] spacings between the topmost layer group V atoms, i.e., the bilayer spacings, can be measured from filled-state STM images, therefore, the resolution of interface transition deduced from [001] atomic bilayer spacings cannot be better than two monolayers.

As shown in Fig. 8, for the GaAs–on–GaAs$_{1-x}$Sb$_x$ interface, the transition from the GaAs$_{1-x}$Sb$_x$ alloy layer to the GaAs layer extends about 6–12 Å (two to four monolayers) in the sample grown with an As soak at the GaAs–on–GaAs$_{1-x}$Sb$_x$ interface, and no more than 6 Å in the sample grown without the anion soak at the interface (one or two monolayers). For the GaAs$_{1-x}$Sb$_x$–on–GaAs interface, the transition from the GaAs layer to the GaAs$_{1-x}$Sb$_x$ alloy layer does not exceed 6 Å (one or two monolayers) in the sample grown with an As+Sb soak at the GaAs$_{1-x}$Sb$_x$–on–GaAs interface, and about 6–12 Å (two to four monolayers) in the sample grown without the interface anion soak. If we recall that the roughness of the As soaked GaAs–on–GaAs$_{1-x}$Sb$_x$ interface is less than that of the untreated GaAs–on–GaAs$_{1-x}$Sb$_x$ interface, and that the As +Sb soak does not significantly affect the roughness of the GaAs$_{1-x}$Sb$_x$–on–GaAs interface, we may conclude that the As+Sb soak at the GaAs$_{1-x}$Sb$_x$–on–GaAs interface most likely improves interface abruptness, while the As soak at the GaAs–on–GaAs$_{1-x}$Sb$_x$ interface may degrade the abruptness of interface.

IV. CONCLUSION

Cross-sectional STM and detailed analysis of STM images have been performed to investigate compositional and interfacial structure within GaAs$_{1-x}$Sb$_x$/GaAs quantum well samples coherently grown on GaAs substrates, with and without group V soaks at the heterojunction interfaces.

Filled-state (110) cross-sectional constant-current images of both samples reveal nanometer-scale compositional features within the GaAs$_{1-x}$Sb$_x$ alloy layers. Both Sb-rich and As-rich regions with irregular shapes as well as compositional features preferentially oriented along the $[\bar{1}12]$ and $[1\bar{1}2]$ directions in the (110) plane are observed. These observations are consistent with theoretical models of surface-induced ordering in epitaxially grown III-V alloy material, and models of nanometer-scale compositional structures formed and evolving under the influence of infinite-range elastic interactions among clusters of varying composition, and between these clusters and the substrate. [001] atomic bilayer spacings extracted from the GaAs$_{1-x}$Sb$_x$/GaAs samples reveal compositional grading along the growth direction within the alloy layer. An algorithm employing analysis of strain-induced surface relaxation and measurement of atomic spacings in STM data is described and used to determine quantitatively the compositional profile within the GaAs$_{1-x}$Sb$_x$ layers in the GaAs$_{1-x}$Sb$_x$/GaAs samples. The Sb composition within the GaAs$_{1-x}$Sb$_x$ alloy layer is found to be significantly graded, ranging from ~30% to ~40%, and from ~27% to ~41%, in the GaAs$_{1-x}$Sb$_x$/GaAs samples grown with and without group V interface soaks,

respectively. These values for Sb composition are consistent with the PL peak energies measured for these samples.

Discrete Fourier analysis of interface profiles extracted from (110) cross-sectional images of the samples grown with and without group V soaks shows the effect of the interface soaks on interface roughness: As soaks reduce the degree of roughness of the GaAs–on–GaAs$_{1-x}$Sb$_x$ interfaces; however, for the GaAs$_{1-x}$Sb$_x$–on–GaAs interface, an As+Sb soak does not seem to affect the interface roughness significantly. [001] atomic bilayer spacings extracted from STM images also reveal the effect of group V soaks on interface abruptness: an As+Sb soak at the GaAs$_{1-x}$Sb$_x$–on–GaAs interface seems to improve interface abruptness, while an As soak at the GaAs–on–GaAs$_{1-x}$Sb$_x$ interface seems to degrade interface abruptness.

[1] E. Yablonovitch and E. O. Kane, J. Lightwave Technol. **6**, 1292 (1988).
[2] W. W. Chow, K. D. Choquette, M. H. Crawford, K. L. Lear, and G. R. Hadley, IEEE J. Quantum Electron. **33**, 1810 (1997).
[3] T. Anan, K. Nishi, S. Sugou, M. Yamada, K. Tokutome, and A. Gomyo, Electron. Lett. **34**, 2127 (1998).
[4] J. F. Klem, O. Blum, S. R. Kurtz, I. J. Fritz, and K. D. Choquette, J. Vac. Sci. Technol. B **18**, 1605 (2000).
[5] H. R. Jen, D. S. Cao, and G. B. Stringfellow, Appl. Phys. Lett. **54**, 1890 (1989).
[6] A. Gomyo, T. Suzuki, and S. Iijima, Phys. Rev. Lett. **60**, 2645 (1988).
[7] D. M. Follstaedt, R. M. Biefeld, S. R. Kurtz, and K. C. Baucom, J. Electron. Mater. **24**, 819 (1995).
[8] K. A. Mäder and A. Zunger, Appl. Phys. Lett. **64**, 2882 (1994).
[9] G. B. Stringfellow and G. S. Chen, J. Vac. Sci. Technol. B **9**, 2182 (1991).
[10] A. Zunger and S. Mahajan, *Handbook on Semiconductors*, Vol. 3B, *Materials, Properties and Preparation*, edited by S. Mahajan (North-Holland, Netherlands, 1994), p. 1399.
[11] P. K. Bhattacharya and J. W. Ku, J. Appl. Phys. **58**, 1410 (1985).
[12] Y.-E. Ihm, N. Otsuka, J. Klem, and H. Morkoç, Appl. Phys. Lett. **51**, 2013 (1987).
[13] H. R. Jen, M. J. Cherng, and G. B. Stringfellow, Appl. Phys. Lett. **48**, 1603 (1986).
[14] H. R. Jen, M. J. Jou, Y. T. Cherng, and G. B. Stringfellow, J. Cryst. Growth **85**, 175 (1987).
[15] H. Chen, R. M. Feenstra, R. S. Goldman, C. Silfvenius, and G. Landgren, Appl. Phys. Lett. **72**, 1727 (1998).
[16] R. L. Nahory, M. A. Pollack, J. C. DeWinter, and K. M. Williams, J. Appl. Phys. **48**, 513 (1977).
[17] A. D. Prints, D. J. Dunstan, J. D. Lambkin, E. P. O'Reilly, A. R. Adams, R. Pritchard, W. S. Truscott, and K. E. Singer, Phys. Rev. B **47**, 2191 (1993).
[18] G. Ji, S. Agarwala, D. Huang, J. Chyi, and H. Morkoç, Phys. Rev. B **38**, 10 571 (1988).
[19] S. L. Zuo, E. T. Yu, A. A. Allerman, and R. M. Biefeld, J. Vac. Sci. Technol. B **17**, 1781 (1999).
[20] G. B. Stringfellow, J. Cryst. Growth **65**, 454 (1987).
[21] J. W. Cahn, Acta Metall. **10**, 179 (1962).
[22] S. Froyen and A. Zunger, Phys. Rev. Lett. **66**, 2132 (1991).
[23] S. Froyen and A. Zunger, Phys. Rev. B **53**, 4570 (1996).
[24] S. B. Zhang, S. Froyen, and A. Zunger, Appl. Phys. Lett. **67**, 3141 (1995).
[25] L. Q. Chen and A. G. Khachaturyan, Phys. Rev. Lett. **70**, 1477 (1993).
[26] L. Q. Chen and A. G. Khachaturyan, Scr. Metall. Mater. **25**, 61 (1991).
[27] L. Q. Chen and A. G. Khachaturyan, Acta Metall. Mater. **39**, 2533 (1991).
[28] L. Q. Chen, Y. Z. Wang, and A. G. Khachaturyan, Philos. Mag. Lett. **65**, 15 (1992).

3770   J. Appl. Phys., Vol. 92, No. 7, 1 October 2002

Zuo *et al.*

[29] R. M. Feenstra, D. A. Collins, D. Z. Y-Ting, M. W. Wang, and T. C. McGill, Phys. Rev. Lett. **72**, 2749 (1994).

[30] A. Y. Lew, S. L. Zuo, E. T. Yu, and R. H. Miles, Phys. Rev. B **57**, 6534 (1998).

[31] J. E. Bernard and A. Zunger, Appl. Phys. Lett. **65**, 165 (1994).

[32] J. C. Woicik, J. G. Pellegrino, S. H. Southworth, P. S. Shaw, B. A. Karlin, C. E. Bouldin, and K. E. Miyano, Phys. Rev. B **52**, R2281 (1995).

[33] T.-L. Lee, M. R. Pillai, J. C. Woicik, G. Labanda, P. F. Lyman, S. A. Barnett, and M. J. Bedzyk, Phys. Rev. B **60**, 13 612 (1999).

[34] T.-L. Lee, M. R. Pillai, J. C. Woicik, G. Labanda, P. F. Lyman, S. A. Barnett, and M. J. Bedzyk, Phys. Rev. B **60**, 13 612 (1999).

[35] J. C. Woicik, Phys. Rev. B **57**, 6266 (1998).

[36] A. Sher, Mark van Schilfgaarde, A.-B. Chen, and W. Chen, Phys. Rev. B **36**, 4279 (1987).

[37] J. Tersoff, R. M. Feenstra, J. A. Stroscio, and A. P. Fein, J. Vac. Sci. Technol. A **6**, 497 (1988).

[38] R. J. Meyer, C. B. Duke, A. Paton, J. L. Yeh, J. C. Tsang, A. Kahn, and P. Mark, Phys. Rev. B **21**, 4740 (1980).

[39] H. M. Tütüncü and G. P. Srivastava, Phys. Rev. B **59**, 4925 (1999).

[40] C. B. Duke, R. J. Meyer, A. Paton, J. L. Yeh, J. C. Tsang, A. Kahn, and P. Mark, J. Vac. Sci. Technol. **17**, 501 (1980).

[41] V. E. De Carvalho, M. Prutton, and S. P. Tear, Surf. Sci. **184**, 198 (1987).

[42] H. M. Tütüncü, M. Çakmak, and G. P. Srivastava, Appl. Surf. Sci. **123/124**, 146 (1997).